

Microstructural evolution and its influence on the magnetic properties of CoFe_2O_4 powders during mechanical milling

B. H. Liu,^{1,2} J. Ding,^{1,*} Z. L. Dong,³ C. B. Boothroyd,⁴ J. H. Yin,¹ and J. B. Yi¹

¹*Department of Materials Science and Engineering, Faculty of Engineering, National University of Singapore, Singapore 117576*

²*Chemistry Department, Faculty of Science, National University of Singapore, Singapore 119260*

³*School of Materials Science and Engineering, Nanyang Technological University, Nanyang Avenue, Singapore 639798*

⁴*IMRE, 3 Research Link, Singapore 117602*

(Received 24 February 2006; revised manuscript received 4 August 2006; published 22 November 2006)

A high coercivity of up to 5.1 kOe was induced in a large-grained CoFe_2O_4 powder after milling for a short time (1.5 h). It was found that the initial grain (particle) size played an important role in the microstructural evolution and in the magnetic properties of the milled CoFe_2O_4 materials. The milling-induced microstructural evolution was analyzed using x-ray diffraction and transmission electron microscopy. The results indicated that the milling-induced high coercivity was associated with the highly-strained and defective microstructure. The enhancement in magnetic anisotropy was observed in large-grained CoFe_2O_4 after milling, which might be mainly attributed to the stress anisotropy. In order to understand the coercivity mechanisms, detailed magnetic studies were carried out by the investigation of the field-dependent magnetization (demagnetization) behaviors and the magnetization reversal processes based on both the micromagnetic model and the phenomenological model. The results revealed that a domain wall pinning-controlled mechanism was responsible for the milling-induced high coercivity in CoFe_2O_4 materials.

DOI: [10.1103/PhysRevB.74.184427](https://doi.org/10.1103/PhysRevB.74.184427)

PACS number(s): 75.50.Vv, 75.50.Gg, 75.60.Jk, 81.40.-z

I. INTRODUCTION

Cobalt ferrite (CoFe_2O_4) is an important hard magnetic oxide because of its potential in many applications, including magnetic data storage, magneto-optical and magneto-electric devices.¹⁻⁴ For hard magnetic applications, coercivity is a key parameter. Although cobalt ferrite possesses a high magnetocrystalline anisotropy,⁵ coercivities obtained in CoFe_2O_4 powdered materials with the cubic spinel structure are usually less than 2 kOe. As it is well known, microstructure plays an important role in coercivity.⁶⁻⁸ We have reported a high coercivity of up to 9.3 kOe in cobalt ferrite thin films.⁹ Such a high coercivity was developed through a careful control of the grain size and the building-up of a relatively large residual strain in the thin film. For powdered cobalt ferrite materials, the highest coercivity achieved so far is 4.6 kOe reported by Chinnasamy *et al.*¹⁰ through controlling the average particle size. Therefore, coercivity enhancement can be realized through controlling the grain (particle) size and/or the establishment of a high level of residual strain inside particles (grains). Many works have reported the importance of microstructure (such as residual stresses) for the coercivity enhancement.^{4,11-16} However, the relationship between microstructure and coercivity has not been well understood for cobalt ferrite.

In this work, mechanical milling was employed as an effective tool to build up a high level of residual strain and a high density of defects in CoFe_2O_4 powders. A high coercivity of up to 5.1 kOe has been achieved after mechanical milling for a relatively short time. We present a detailed study on the microstructural evolution during mechanical milling and its effect on the magnetic properties (coercivity and saturation magnetization) of CoFe_2O_4 powders. In order to understand the mechanisms behind the milling-induced high coercivity, detailed magnetic studies were carried out based on

both the micromagnetic model and the phenomenological model. Our study revealed that the domain-wall pinning mechanism was responsible for the magnetization and demagnetization processes in the mechanically milled CoFe_2O_4 powders with high coercivities.

II. EXPERIMENTAL DETAILS

CoFe_2O_4 precursor powders were prepared by the conventional coprecipitation method at room temperature. After thorough washing, the as-obtained precursors were annealed at different temperatures to obtain the well crystallized spinel phase (CoFe_2O_4). In order to investigate the effect of initial particle (grain) size on the microstructure evolution, three CoFe_2O_4 powders were used as the starting materials for mechanical milling in this work, namely powders annealed at 300 °C (denoted as powder A), annealed at 1000 °C (denoted as powder B), and annealed at 1300 °C (denoted as powder C). Mechanical milling was conducted in a Spex-8000 high-energy miller with a 12:1 weight ratio of ball to powder. The three powders were mechanically milled and sampled for different periods of time up to 36 h. The phases, the grain size, and residual strain of milled samples were analyzed by x-ray diffraction (Bruker XRD with Cu $K\alpha$ radiation). The diffraction patterns were collected using θ - 2θ scanning with the step size of 0.02°. The divergence, anti-scattering, and detector slits were 0.1°, 0.1°, and 0.1 mm, respectively, in the XRD study. The separation of the line broadenings due to the grain-size effect and the strain effect of XRD diffraction peaks was based on the Williamson-Hall plot.¹⁷ The microstructure of the milled samples was examined using different transmission electron microscopy (TEM) imaging and diffraction techniques with a JEOL JEM 3010 TEM operated at 300 kV. For the TEM sample preparation, the large-grained powdered specimens (powder B and pow-

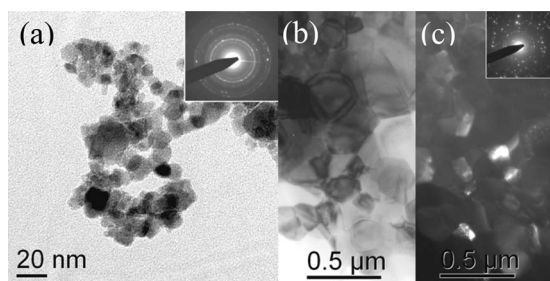


FIG. 1. (a) Bright-field TEM image and electron diffraction pattern (inserted) of powder A; (b) bright-field and (c) dark-field TEM image and electron diffraction pattern (inserted) of powder B before mechanical milling.

der C before milling and after milling for a short time) were first mixed with epoxy resin and then thinned by polishing and ion-milling. For small-grained samples such as powder A and the samples after milling for a long time, particles were first dispersed in ethanol and then dropped on the carbon-coated Cu grids. A VSM (vibration sample magnetometer, Oxford) was used for magnetic measurements, including magnetic viscosity, minor loops, and dc demagnetization curves. ^{57}Fe (^{57}Co in a Rh matrix) Mössbauer spectroscopy (FAST ComTec, Germany) was used for the analysis of the site occupation of the magnetic ions in the CoFe_2O_4 spinel lattice before and after mechanical milling. A spectrum of metallic bcc-Fe was used for the calibration. Low temperature Mössbauer measurements were conducted in a liquid nitrogen cryostat. Spectra were analyzed with a computer program (RECOIL). The area ratio of tetrahedral (*A* site) to octahedral (*B* site) subspectra was used for determination of the cation distribution.

III. RESULTS

A. Starting materials

XRD analysis indicated that all the samples are of the spinel (CoFe_2O_4) phase after annealing at different temperatures. The magnetic properties of annealed samples, coercivity (H_C) and magnetization (M_S), are listed in Table I. Our

TABLE I. The saturation magnetization and coercivity of CoFe_2O_4 samples after annealing.

| Annealing temperature (°C) | Saturation magnetization, M_S (emu/g) | Coercivity, H_C (Oe) |
|----------------------------|---|------------------------|
| 0 | 56.8 | 660.5 |
| 300 | 67.6 | 876.2 |
| 600 | 71.6 | 968.6 |
| 800 | 79.4 | 1092.3 |
| 1000 | 81.7 | 1230.4 |
| 1300 | 83.6 | 680.5 |

Mössbauer analysis confirmed the single spinel phase. For all the three starting powders (powder A, B, and C) before mechanical milling, the Mössbauer analysis at 80 K indicates that the ratio of Fe^{3+} ions at *A* site to *B* site was close to 1:1, corresponding to the inverse spinel structure ($\text{Fe}_{A\text{-site}}[\text{CoFe}]_{B\text{-site}}\text{O}_4$). The change of H_C with annealing temperature in Table I can be ascribed to the effect of the grain (particle) size.^{18,19} The results were consistent with those published previously,²⁰ which reported that CoFe_2O_4 powdered materials usually possess relatively low coercivities in the range of 1–2 kOe. The low M_S value of powder A could be attributed to finite-size effects such as surface spin disordering (canting), as often found in nanoparticle materials.²¹ The M_S values of 81 and 83 emu/g for powder B and powder C are close to the theoretical value (80 emu/g) for bulk CoFe_2O_4 .²² The coercivity was 0.87 kOe, 1.23 kOe, and 0.68 kOe for powder A, powder B, and powder C, respectively.

For powder A, annealing at 300 °C did not lead to a significant grain growth and the particle size remained in the nanosize range (10–20 nm), as indicated by the bright-field TEM image shown in Fig. 1(a). The inset selected-area electron diffraction pattern in Fig. 1(a) shows the polycrystalline structure. For powder B and powder C, micrometer-sized particles were observed under TEM, as shown in Figs. 1(b) and 1(c) for powder B. The agglomeration of submicrometer-sized grains indicates that the severe grain growth and sin-

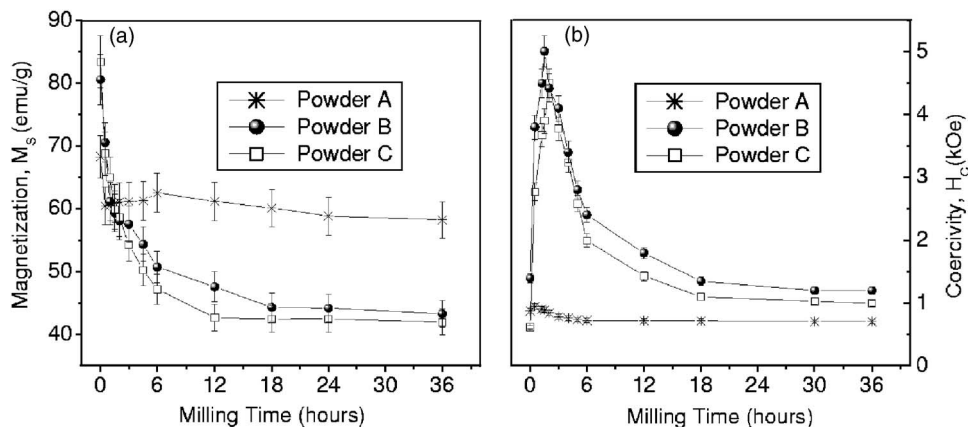


FIG. 2. Variation of (a) saturation magnetization (M_S) and (b) coercivity (H_C) of powder A, powder B, and powder C with mechanical milling time.

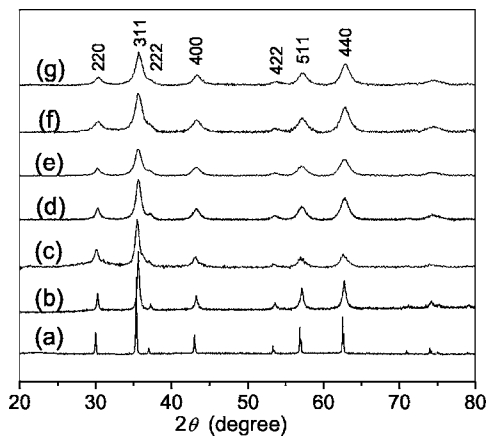


FIG. 3. XRD spectra of powder B before milling and after milling for different periods of time: (a) as annealed at 1300 °C before milling; (b) as milled for 30 min; (c) as milled for 90 min; (d) as milled for 3 h; (e) as milled for 6 h; (f) as milled for 12 h; (g) as milled for 18 h.

tering occurred when the samples were annealed at 1000 °C and 1300 °C. The inserted spotty diffraction rings in the diffraction patterns also suggested the large-grained microstructure. Based on the dark-field TEM analysis, the estimated average grain sizes were around 12 nm, 240 nm, and 340 nm for powder A, powder B, and powder C, respectively, consistent with the results of the XRD analysis.

B. Milled CoFe_2O_4 powders

1. Milling-time dependent magnetic properties

Figures 2(a) and 2(b) show the room-temperature saturation magnetization M_S and coercivity H_C of the three powders after mechanical milling for different periods of time. Compared to powder B and C, powder A showed relatively smaller reduction in M_S (from approximately 68 emu/g to 57 emu/g), and its H_C remained nearly unchanged with mechanical milling up to 36 h. Powder B and powder C had a similar trend for the change in M_S and H_C , as shown in Figs. 2(a) and 2(b). For both powder B and C, M_S continuously decreased initially and then gradually reached the final value after a prolonged milling (from 80–85 emu/g initially to 40–45 emu/g after milling over 20 h). The H_C of both samples increased rapidly initially and reached the maximum values after a short milling time (5.1 kOe after milling for 1.5 h for powder B and 4.6 kOe after milling for 2 h for powder C). Further milling led to a decrease in H_C , which finally reached values of around 1 kOe after a prolonged milling for both samples. The results suggest that the initial grain (particle) size of the raw materials may play an important role in the change of magnetic properties of the samples during mechanical milling.

2. XRD analysis

For powder A, no apparent changes in the XRD spectra (peak shift and line broadening) were observed and also no other phases were detected in the samples after mechanical

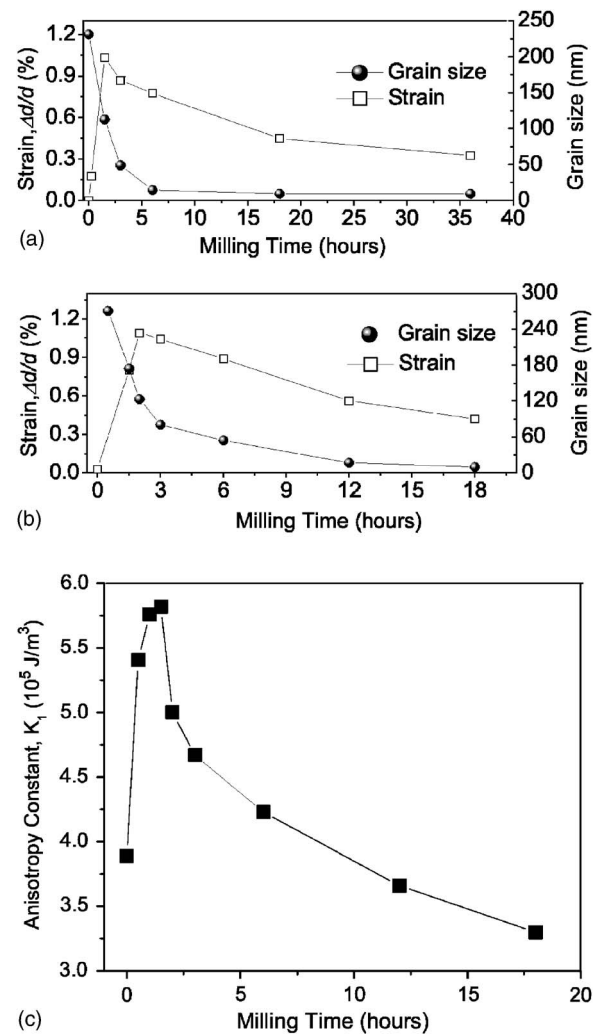


FIG. 4. Variation of strain and average grain size of (a) milled powder B and (b) powder C with mechanical milling time; (c) variation of the magnetic anisotropy constant of powder B with mechanical milling time.

milling for up to 36 h. The Williamson-Hall plots¹⁷ revealed that no strain in samples (powder A) before and after mechanical milling was present and the average grain size remained almost unchanged after milling.

Figure 3 shows the XRD spectra of powder B before milling and after milling for different periods of time. With the progress of mechanical milling, diffraction line broadening was observed. Based on the Williamson-Hall plot analysis, the average grain size and the residual strain were calculated for powder B before and after milling, as plotted in Fig. 4(a). As seen in Fig. 4(a), the change in residual strain was quite similar to that of H_C with milling time as shown in Fig. 2(b). The results indicate that the highest H_C corresponds to the largest residual strain (around 1.03%) which appeared after milling for 1.5 h. The results suggest that the high coercivity is closely related to the large residual strain induced by mechanical milling. For powder C before and after milling, XRD spectra showed similar patterns to Fig. 3. The milling-induced high-level residual strain was also detected in the milled powder C as indicated in Fig. 4(b). The change of

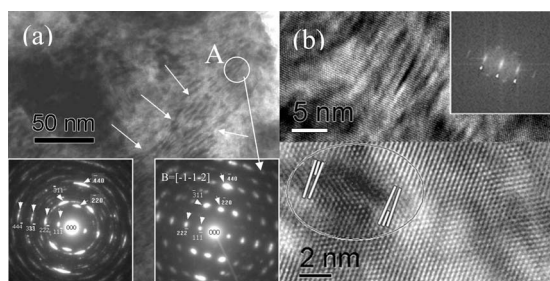


FIG. 5. (a) Bright-field TEM image with selected-area electron diffraction and nanobeam diffraction patterns, and (b) high-resolution TEM images of powder B milled for 1.5 h.

residual strain also agreed with the change in H_C , as found in powder B after mechanical milling.

On the other hand, the mechanical milling resulted in an apparent grain refinement for both powder B and powder C as indicated in Figs. 4(a) and 4(b). The milled powder B with the highest coercivity had an average grain size of 110 nm, while milled powder C with the highest coercivity had an average grain size of 123 nm. As discussed previously (Table I), relatively low coercivities (<1.3 kOe) were found in the annealed CoFe_2O_4 powders, when the grain size was in the range of 12–340 nm. The milling-induced high coercivities were much higher than those of the annealed samples with similar grain sizes. These results indicated that the grain size effect does not play a major role in the high coercivity.²³

3. TEM analysis

For powder A, bright-field TEM analysis indicated no apparent change in morphology after milling for up to 36 h, when compared with the sample before mechanical milling [Fig. 1(a)]. Dark-field TEM analysis revealed no apparent change in average grain size after mechanical milling for up to 36 h. The results imply that prolonged mechanical milling did not induce appreciable microstructural changes in powder A.

Before mechanical milling, powder B possessed a well-crystallized structure with few defects as indicated by the high-resolution TEM analysis. The uniform contrast inside each grain and along grain boundaries in TEM images may indicate a low strain level in the sample. After mechanical milling for 1.5 h, microcracks were observed under TEM, suggesting the fracture induced by the short-time high-energy mechanical milling. In addition, many defects were seen inside each grain (particle) in both dark field and bright field due to their strain fields. The bright-field TEM image in Fig. 5(a) indicates the formation of distorted bands as shown by arrows. These bands are so-called shear bands as often observed in mechanically-milled materials.^{24–26} The formation of subgrains inside particles or the “parent” grains took place, as verified by selected-area electron diffraction inserted in Fig. 5(a) [taken from the large particle in Fig. 5(a)], revealing a textured polycrystalline structure of the large particle. The inserted nanobeam diffraction pattern (taken from the circled area A) indicates that textured grains are present with a similar orientation with respect to each other. Figure 5(b) shows HRTEM images of the shear bands, revealing the

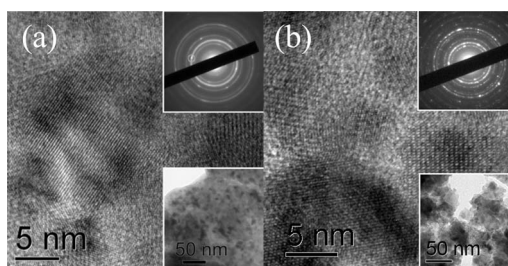


FIG. 6. (a) High-resolution TEM images of powder B milled for (a) 6 h and (b) 36 h (inserted are bright-field TEM images and the selected-area electron diffraction patterns).

strong distortion of these shear bands. The diffractogram from these irregular shear bands indicates double diffraction along a preferred orientation, which suggests that these shear bands are actually moiré fringes. The distortion of the shear bands could be ascribed to the existence of defects such as dislocations inside. Within these shear bands, many dislocations were observed. The associated strong strain contrast indicates a high-level strain in this sample. These results indicate that a highly strained defective structure was formed after mechanical milling for the relatively short time of 1.5 h. Further mechanical milling for up to 6 h readily led to the formation of many nanosized subgrains inside the parent grains (particles). As shown in Fig. 6(a), nanocrystals were formed with well distinguished grain boundaries. Some regions between the grain boundaries had a disordered or amorphous-like structure. The selected-area electron diffraction pattern (inserted) also indicates the polycrystalline structure and the loss of the texture relationship among these grains. Prolonged mechanical milling for up to 36 h resulted in significant grain refinement as indicated by the TEM analysis as shown in Fig. 6(b). The high-resolution TEM analysis suggests the formation of nanosized grains with an amorphous phase at the grain boundaries.

For powder C, similar microstructures as for powder B were observed under TEM after milling for 2 h, 6 h, and 36 h. This indicates that powder B and powder C underwent similar microstructure evolution during mechanical milling.

IV. DISCUSSION

A. Milling-induced microstructural evolution and its effects on magnetic properties

For powder A with a nanocrystalline structure, as mentioned above, both structural and magnetic analysis suggest that mechanical milling did not induce significant changes in either microstructural or magnetic properties. It is recognized that, in very small crystals, the formation and the movement of the dislocations require very high strain energy, which hinders the deformation of nanograins.^{24,27,28} This may well explain why powder A did not show apparent structural changes even after prolonged milling for up to 36 h. The decrease in M_S with milling might be due to the small amount of large particles in the starting powders before mechanical milling. Since no compositional and microstructural changes were induced by mechanical milling, it is expected

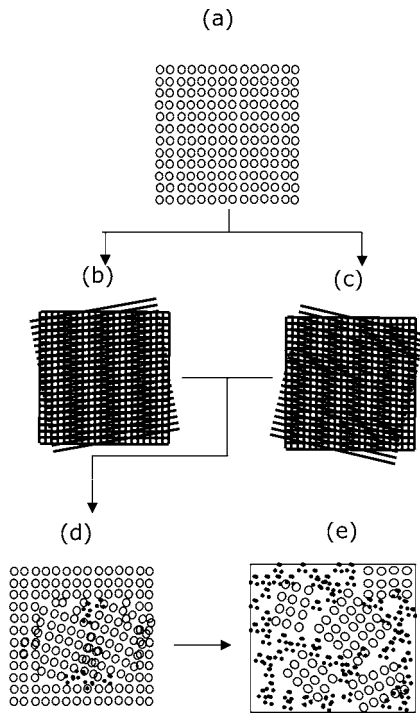


FIG. 7. Schematic illustration of the proposed microstructure evolution of CoFe_2O_4 powders with large grain size during mechanical milling: (a) before milling; (b) and (c) the initial stage of milling; (d) the intermediate stage of milling; (e) the final stage for the formation of nanocrystalline microstructure after prolonged milling.

that the coercivity H_C of powder A did not show apparent changes with milling.

For large-grained CoFe_2O_4 samples such as powder B and powder C, apparent microstructural changes were induced by mechanical milling. Based on XRD and TEM analysis as mentioned above, we suggest that the microstructure evolution of large-grain CoFe_2O_4 powders can be illustrated by Fig. 7, namely, (i) the initial stage with the formation of textured subgrains accompanied by the introduction of high-level strain and high-density defects; (ii) the intermediate stage with the formation of subgrains with the loss of texture and the decrease in both microstrain and defect density; (iii) the final stage with the formation of the final nanostructure.

At the initial stage of milling, typically with a milling time of several hours, the high-energy milling induced a highly strained defective microstructure accompanied by the formation of subgrains inside the parent grains (particles). The defective microstructure was evidenced by the formation of distorted shear bands within which bountiful dislocations were observed. It was reported that the development of shear bands was responsible for the formation of subgrains during mechanical milling with the accumulation of dislocations.^{24–26} Therefore, the development of distorted shear bands signals not only the formation of subgrains but also the accumulation of defects. The strong lattice distortion and strain contrast associated with distorted shear bands may suggest the presence of high-level strain inside the sample. In addition, TEM analysis revealed textured structures among the subgrains, implying milling-induced gliding or

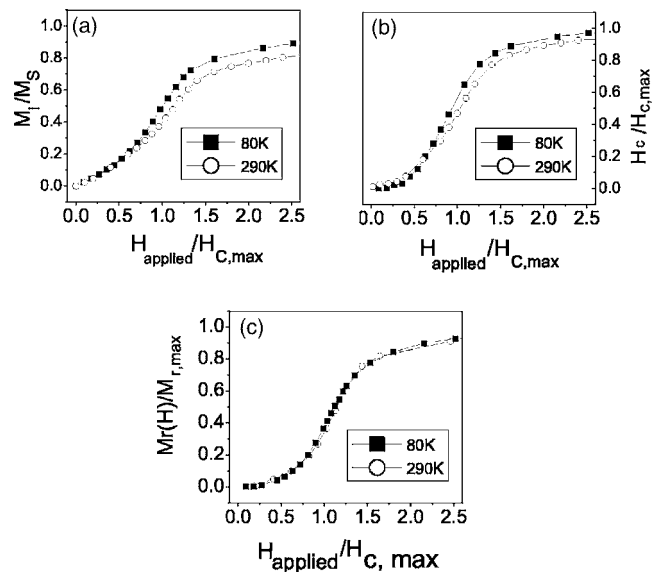


FIG. 8. The normalized field-dependent (a) initial magnetization $[M_i(H)]$, (b) coercivity $H_C(H)$, and (c) remanence $[M_r(H)]$ of powder B milled for 1.5 h at 80 K and 290 K (H_{applied} : applied field; $H_{C,\text{max}}$: the saturation coercivity measured at 60 kOe; $M_{r,\text{max}}$: the saturation remanence).

rotation between subgrains or between subgrains and parent grains at this initial milling stage. Therefore, in areas with fewer defects, the slight misorientation between the subgrains led to the formation of more regular moiré fringes as illustrated in Fig. 7(b); while where there were many defects, distorted moiré fringes appeared as illustrated in Fig. 7(c). At this initial milling stage, both the magnetization (M_S) and the coercivity (H_C) of the milled samples underwent appreciable changes. A rapid decrease in the M_S was observed, which could be ascribed to structural disordering and/or the partial amorphization at the grain boundaries. A rapid decrease in M_S with a short milling time was also observed in mechanically milled SmCo_5 .²⁹ The milling-induced high coercivity at this milling stage could be related to the formation of a defective structure with high-level strain and high-density defects as mentioned above, which will be discussed in detail later.

During the intermediate milling stage, further grain refinement occurred due to the accumulation of milling-induced defects, as for the samples milled for 6 h. Increased structure disordering (amorphization) near grain boundaries was observed, which may lead to strain release as indicated by XRD analysis. In addition, the loss of the texture and the formation of high-angle grain boundaries indicate that the subgrains were highly misoriented, which was verified by high-resolution TEM and electron diffraction. The structure formed at this stage can be illustrated by Fig. 7(d). The decrease in M_S at this milling stage could be ascribed to structural disordering and the formation of appreciable amounts of nanograins. The decrease in H_C could be due to the release of residual strain and the decrease in the defect density as well as the formation of nanograins that may appear superparamagnetic at room temperature.

At the final milling stage, prolonged mechanical milling led to continuous grain refinement and finally a stationary

microstructure was reached, namely the formation of randomly oriented nanograins with amorphous-like phases in the region of grain boundaries, as illustrated by Fig. 7(e). The achievement of such a final nanostructure could be due to the balance between the milling-induced strain energy and the high surface energy of CoFe_2O_4 nanograins.²⁴ Hence further milling will not lead to further microstructural changes. In this study, the sample milled for 36 h was close to the final milling stage, as indicated by high-resolution TEM analysis. Given the finite-size effects of nanocrystalline materials and the low magnetization and magnetic anisotropy of disordered materials,¹⁷ the low values of M_S and H_C of the samples milled for 36 h are reasonable.

B. Mechanism of milling-induced high coercivity

1. Magnetic anisotropy

Using the law of approach to saturation,³⁰ we estimated the magnetic anisotropy constant K_1 of the milled powder B. According to Ref. 30, if K_2 is ignored, the cubic anisotropy function can be expressed as

$$M(H) = M_S \left(1 - \frac{0.07619K_1^2}{H^2M_S^2} - \frac{0.0384K_1^3}{H^3M_S^3} \right), \quad (1)$$

where $M(H)$ is the magnetization at an applied field of H and M_S is the saturation magnetization. The K_1 can be estimated by fitting $M(H)$ - H curves at a certain field range. The estimated K_1 (more accurately, the effective anisotropy constant in this case) is shown in Fig. 4(c). Clearly, the change of K_1 was consistent with that of H_C as shown in Fig. 2(b), i.e., the highest H_C corresponded to the highest anisotropy constant. It indicates that the sample milled for 1.5 h possessed an enhanced magnetic anisotropy, around $5.8 \times 10^5 \text{ J/m}^3$, which is approximately 50% higher than that of the sample before milling. The enhanced magnetic anisotropy may have two possible contributions: (i) the change in the site occupation of magnetic ions due to mechanical milling; (ii) the stress anisotropy due to the milling-induced high-level strain.

It has been recognized that the high magnetocrystalline anisotropy of CoFe_2O_4 arises from the incompletely quenched orbital momentum of Co^{2+} at the octahedral sites in the spinel lattice. Therefore, the change in cation distribution may lead to the change in the magnetocrystalline anisotropy and thus magnetic coercivity. Milling-induced cation redistribution has been reported in ferrite materials, such as ZnFe_2O_4 (Ref. 31) and MgFe_2O_4 .³² In order to examine whether mechanical milling could induce a cation redistribution in CoFe_2O_4 samples after milling, Mössbauer spectroscopy was used in this work. For the milled samples, the Mössbauer spectra at 80 K became broadened. The fitting results revealed no significant changes in cation distribution after milling for powder A. For powder B milled for 1.5 h, the fitting results showed that the absorption area ratio of A-site to B-site subspectra was changed 0.92/1.08, indicating that a small amount of Co^{2+} ions have migrated from B sites to A sites. As the magnetocrystalline anisotropy of CoFe_2O_4 arises mainly from the contribution of Co^{2+} on the B sites, the milling-induced migration of Co^{2+} from B to A sites may

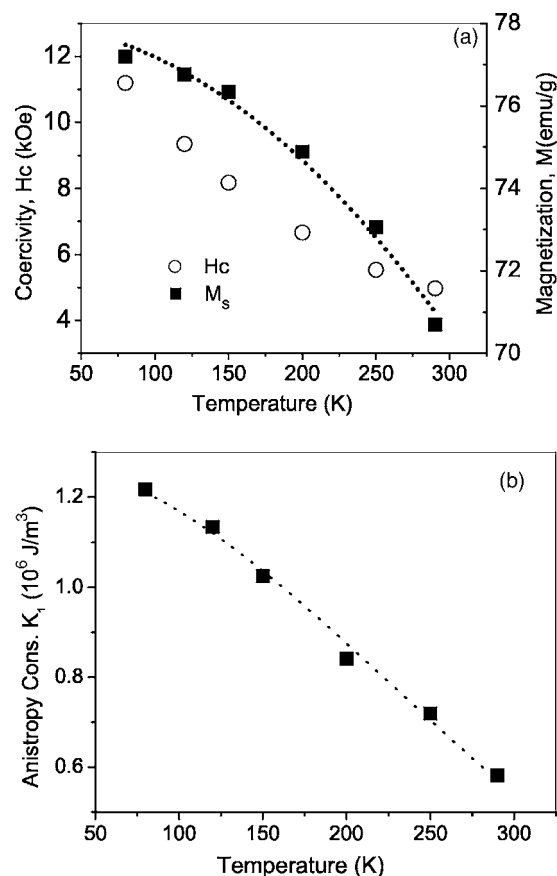


FIG. 9. (a) Temperature-dependent coercivity (H_C) and saturation magnetization (M_S) as well as (b) magnetic anisotropy (K_1) of powder B milled for 1.5 h (symbols: experimental data; dotted line: fitting curves).

decrease the magnetocrystalline anisotropy in CoFe_2O_4 , as reported previously.³³ Therefore, the milling-induced enhancement in the magnetic anisotropy in Fig. 4(c) might be mainly resulted from other mechanisms, such as the stress anisotropy.

In terms of magnetoelastic theory, the residual strain may induce additional uniaxial magnetic anisotropy, i.e., stress anisotropy K_S which is given by $K_S = 3/2\lambda\sigma$ in case of isotropic magnetostriction (λ is the magnetostriction constant and σ is the stress which is proportional to strain via Young's modulus Y). For polycrystalline CoFe_2O_4 materials, the average magnetostriction constants λ is -1.1×10^{-4} (Ref. 34) and Young's modulus Y is $142 \times 10^9 \text{ Pa}$ (i.e., $1.42 \times 10^{11} \text{ N/m}^2$).³⁵ Therefore, the estimated stress anisotropy K_S of powder B milled for 1.5 h (with a strain of $\sim 1.03\%$ estimated from XRD) is calculated to be $2.4 \times 10^5 \text{ J/m}^3$. Given the magnetocrystalline anisotropy K_1 of $3.8 \times 10^5 \text{ J/m}^3$ of powder B before milling, the effective anisotropy K_{eff} of the sample after milling could be $K_{eff} = \sqrt{K_1^2 + K_S^2}$,³⁶ i.e., $4.5 \times 10^5 \text{ J/m}^3$. This value is in the same order as that estimated by the law of approach to saturation in Fig. 4(c). Based on the above discussion, the enhanced magnetic anisotropy observed in powder B milled for 1.5 h could be mainly attributed to the stress anisotropy.

It is interesting to note that the coercivity increased from 1.23 kOe (before the milling) to 5.1 kOe after milling for

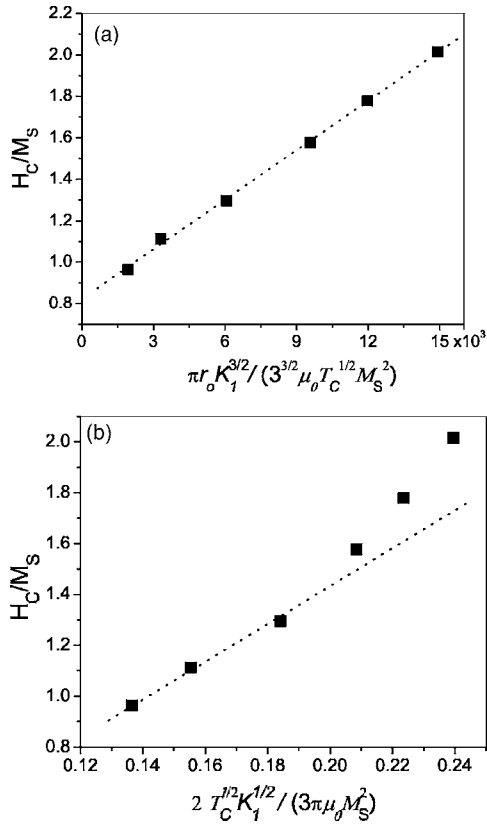


FIG. 10. (a) Test of pinning-controlled coercivity mechanism with $r_0 < \delta_B$; (b) test of pinning-controlled coercivity mechanism with $r_0 > \delta_B$ for powder B as milled for 1.5 h.

1.5 h for powder B (corresponding to an increase rate of 360%), while the increase of anisotropy was approximately 50% (from 3.8 to 5.8×10^3 J/m³). Therefore, besides the stress anisotropy, other factors may also have an important contribution to the large increase of coercivity. As it is well known, the defects and residual strain may play as pinning centres to enhance the coercivity.^{6-8,11,37-40} In order to examine the pinning-controlled mechanism, we choose the milled powder B with the highest coercivity for the detailed investigation.

2. The initial magnetization and the field-dependent coercivity and remanence of milled powder B

The examination of the initial magnetization behavior of hard magnetic materials can provide useful information on magnetic hardening mechanisms.¹¹ Figure 8(a) shows the initial magnetization $M_i(H)$ curves of powder B milled for 1.5 h at both 80 K and 290 K. Apparently, at both temperatures, the initial magnetization increased slowly at low applied field, and increased fast when the applied field reached a level comparable to the intrinsic coercive field, $H_{C,max}$. Similar behavior was observed for the demagnetization processes of the sample, as indicated by the field dependent remanence $M_r(H)$ and coercivity $H_c(H)$ in Figs. 8(b) and 8(c), respectively. This type of magnetization and demagnetization behavior can be generally described as indicators of a domain-wall pinning mechanism.^{6-8,11,37-40} In addition,

there was not much difference in the field dependence of the M_i , H_C and M_r curves at 290 K and 80 K, suggesting then similar magnetic hardening mechanisms at both temperatures.

3. Examination of the pinning-controlled coercivity mechanism based on the micromagnetic model

According to the micromagnetic model, in case of the pinning controlled magnetization, the temperature-dependent coercivity $H_C(T)$ can be described as a function of K_1 (magnetic anisotropy), M_S (saturation magnetization), δ_B (domain wall width), and r_0 (the size of magnetic inhomogeneities).^{6-8,41,42} Considering the temperature dependence of K_1 , M_S , and δ_B ($\delta_B \sim T_C^{1/2}/K_1^{1/2}$, where T_C refers to the Curie temperature and K_1 the magnetic anisotropy constant⁴²), the temperature dependent coercivity $H_C(T)$ can be expressed by Eqs. (2) and (3):

$$\frac{H_C(T)}{M_S(T)} = b \frac{\pi r_0 K_1^{3/2}(T)}{3\sqrt{3}\mu_0 T_C^{1/2} M_S^2(T)} - N_{eff}, \quad \text{if } r_0 < \delta_B, \quad (2)$$

and

$$\frac{H_C(T)}{M_S(T)} = c \frac{2T_C^{1/2} K_1^{1/2}(T)}{3\pi r_0 \mu_0 M_S^2(T)} - N_{eff}, \quad \text{if } r_0 > \delta_B, \quad (3)$$

where b and c are constants, and N_{eff} refers to the demagnetization factor. The $H_C(T)$ and $M_S(T)$ can be experimentally obtained as shown in Fig. 9(a), while the temperature dependent $K_1(T)$ was derived by using the law of approach to saturation as mentioned above. For powder B milled for 1.5 h, the estimated temperature-dependent magnetic anisotropy $K_1(T)$ is plotted out in Fig. 9(b). According to the $K_1(T)$ function reported,⁴⁴ fitting the experimental data in Fig. 9(b) led to

$$K_1(T) = 1.29 \times 10^6 \times \exp(-1.0 \times 10^{-5} T^2) \text{ J/m}^3, \quad (4)$$

which is close to the $K_1(T)$ function reported in Ref. 44. Figures 10(a) and 10(b) show two plots for testing these two pinning models as described by Eqs. (2) and (3), respectively. It follows from a good linear relation between $H_C(T)/M_S(T)$ and $\pi K_1^{3/2}(T)/3\sqrt{3}\mu_0 T_C^{1/2} M_S^2(T)$ as shown in Fig. 10(a) that the coercivity is controlled by the magnetic inhomogeneities with the size smaller than the domain wall width, namely $r_0 < \delta_B$. This could be reasonable and consistent with the results of our TEM analysis by which a high density of dislocations was observed in this sample. It is possible that these low-dimensional defects act as the effective pinning centers for the hindrance of domain wall movement. Fitting the data in Fig. 10(a) gave rise to N_{eff} of around 0.8235 which is reasonable. However, due to the unknown constant b , the estimation of r_0 is impossible.

4. Examination of the coercivity mechanism based on the phenomenological model

To further confirm the pinning-controlled coercivity mechanism, we examined the magnetization reversal of powder B milled for 1.5 h based on a phenomenological model.

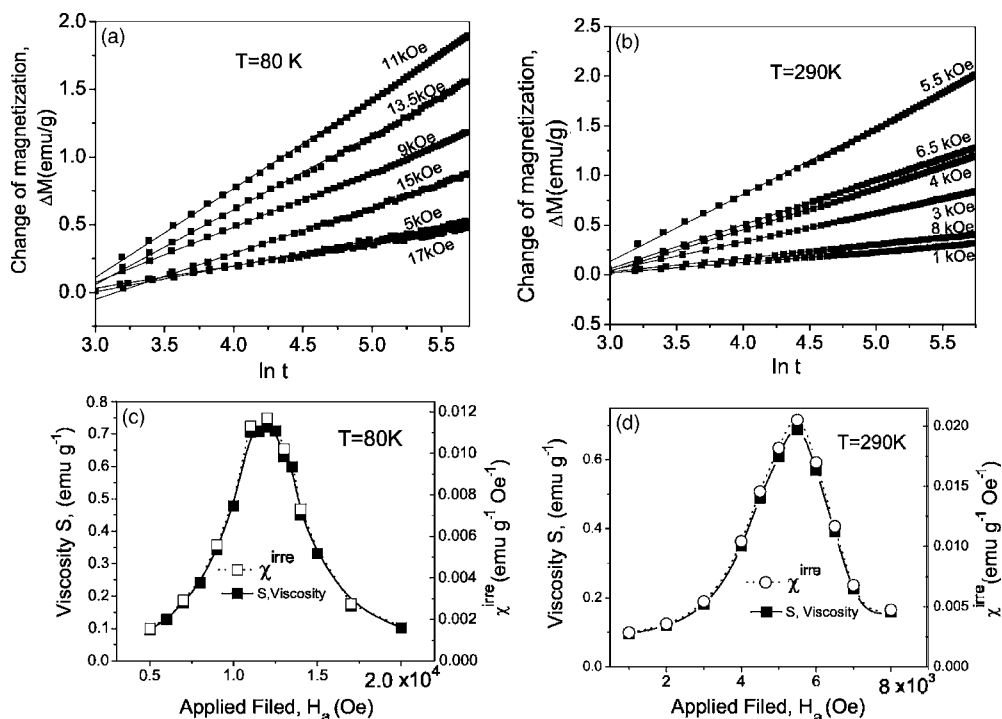


FIG. 11. Time-dependent magnetization curves at (a) 80 K and (b) 290 K, and field dependent magnetic viscosity (S) and irreversible susceptibility (χ^{irre}) at (c) 80 K and (d) 290 K for powder B milled for 1.5 h.

As it is well known, the thermal activation volume (v_a) associated with magnetic relaxation processes can provide useful information on coercivity mechanisms of hard magnetic materials.^{11,45–48}

Based on the work of Barbier⁴⁹ and Wohlfarth,⁴⁶ Liu and Luo³⁸ proposed the relationship between the temperature-dependent $H_C(T)$ and the thermal activation volume $v_a(T)$ as $\log H_C(T) = \log v_a^{-1}(T) + b(T)$, where $b(T)$ is a function of temperature which characterizes the mechanisms of the magnetization reversal processes. Thus, the temperature-dependent $b(T)$ can be obtained through the measurement of $H_C(T)$ and $v_a(T)$. While $H_C(T)$ can be measured straightforwardly, $v_a(T)$ has to be deduced based on the equation $v_a = \frac{kT\chi^{irre}}{M_S S}$ (where kT , M_S , χ^{irre} , and S refer to Boltzmann's energy, saturation magnetization, irreversible magnetic susceptibility, and magnetic viscosities).^{45–48} The magnetic viscosity S can be derived from the time-dependent magnetization $M(t)$ at different field strengths and different temperatures,^{45–48} and χ^{irre} can be obtained from the dc demagnetization curves.

For powder B milled for 1.5 h, the field dependent magnetic viscosities (S) and the irreversible magnetic susceptibilities (χ^{irre}) were obtained at different temperatures from 80 K to 290 K. Figures 11(a)–11(d) show the plots of the time-dependent magnetization curves and S as well as χ^{irre} measured at 80 K and 290 K. Based on the equation of $v_a = \frac{kT\chi^{irre}}{M_S S}$, the temperature-dependent thermal activation volume v_a is calculated and plotted in Fig. 12. Apparently, the activation volume decreased with decreasing temperature, implying a decrease in the size of the active regions that were responsible for the thermal activated magnetization re-

versal processes. At room temperature, the thermal activation volume v_a is around 3100 nm^3 , which is comparable to the volume of a small spherical grain of 9 nm in diameter, apparently smaller than the average grain size, 110 nm as estimated by XRD analysis as mentioned above. In terms of physics of the pinning controlled magnetization, the thermal activation volume v_a could be the volume of material which is covered by a single jump between pinning centers of a domain wall after thermal activation⁴⁶ or the volume associated with the magnetization change between the maximum and minimum energy positions of a domain wall or the maximum and minimum magnetization orientations in a single domain,⁴⁷ or the volume related to pinning sites.⁴⁸ Whichever is true, the small activation volume v_a in this study may suggest that domain walls cannot propagate freely through the inner part of the grains, and were probably pinned by the

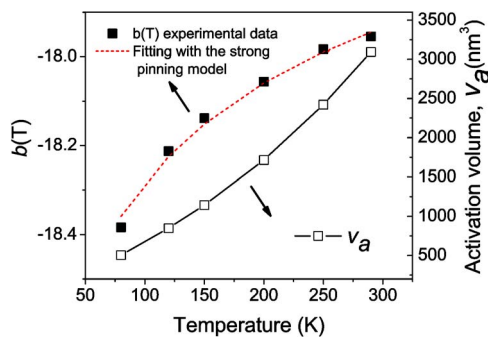


FIG. 12. (Color online) Temperature dependence of activation volume, v_a (denoted by scatters: \square), $b(T)$ [denoted by scatters: \blacksquare] of powder B milled for 1.5 h [the dotted curve was the $b(T)$ curve fitted with the strong pinning model].

pinning sites inside the grains. According to the high resolution TEM analysis as mentioned above, mechanical milling for 1.5 h has induced a highly defective structure in CoFe₂O₄ materials with a high level of strain and a high density of dislocation-type defects. These dislocations inside grains could be active pinning centers that are responsible for the hindrance of domain wall movement.

The activation volume v_a drops rapidly with falling temperature. It could be understood in terms of the temperature dependence of the pinning force at the pinning centers. As pointed out by Chen and Gaunt,⁵⁰ the pinning force f at a pinning site is linearly proportional to $K_1^{3/2}/A^{1/2}$, namely $f = aK_1^{3/2}/A^{1/2}$, where a , K_1 , and A are a constant, the anisotropy constant and exchange constant, respectively. Since A is proportional to the Curie temperature T_C ,⁴³ the pinning force f can be written as $f = aK_1^{3/2}/T_C^{1/2}$, where a is a constant. Because T_C is a constant and K_1 increases as the temperature decreases, it is expected that the pinning force increases as the temperature decreases. Therefore, some pinning sites that are weak at room temperature can be “activated” at low temperatures due to their increased pinning force. This leads to either an increase in the density of pinning sites or a decrease in the size of the pinning sites with an averaging out the size of all pinning sites. Therefore, the thermal activation volume v_a will decrease as the temperature decreases as shown in Fig. 12. Based on the experimentally obtained values of $H_C(T)$ and $v_a(T)$, the temperature dependent $b(T)$ is shown by the squares in Fig. 12.

As given in Ref. 38, for the strong pinning model, $b(T)$ can be expressed as

$$b(T) = \lg \left\{ \frac{75kT}{4M_S} \left[\left(\frac{4f\delta_B}{75kT} \right)^{2/3} - 1 \right] \right\}, \quad (5)$$

where k , T , M_S , f , and δ are Boltzmann’s constant, absolute temperature, spontaneous magnetization, the maximum pinning force from a single pin, and domain wall width, respectively. Considering $\left(\frac{4f\delta}{75kT}\right)^{2/3} \gg 1$,^{38,51} $f = aK_1^{3/2}/T_C^{1/2}$, and $\delta_B = c\frac{T_C^{1/2}}{K_1^{1/2}}$, Eq. (5) can be expressed as

$$b(T) \approx \lg \left(c \frac{(T^{1/3}K_1^{2/3}(T))}{M_S(T)} \right), \quad (6)$$

where c is a constant. If the coercivity mechanism of the powder B milled for 1.5 h can be described by the strong

pinning model, then the experimentally obtained $b(T)$ can be well fitted by the function shown in Eq. (6).

The temperature dependence of M_S was shown in Fig. 9(a) and the as-fitted function of $M_S(T)$ was

$$M_S(T) = 78.02 - 8.0 \times 10^{-5}T^2 \text{ emu/g}, \quad (7)$$

which follows the similar function as reported for CoFe₂O₄ materials.⁵² After all the units were converted into SI units, and Eqs. (4) and (7) were combined, the temperature dependence of $b(T)$ was fitted with Eq. (6). The as-fitted curve is shown in Fig. 12. As seen from Fig. 12, the good fit suggests that the strong pinning model can describe the coercivity mechanism in powder B as milled for 1.5 h well. This is consistent with analysis based on both the micromagnetic model and the field-dependent magnetization and demagnetization behaviors.

V. CONCLUSION

Mechanical milling was demonstrated to be an effective way for introducing a high level of strain and a high density of defects in CoFe₂O₄ powdered materials. A high coercivity of up to 5.1 kOe was induced by milling large-grained CoFe₂O₄ powders for a relatively short time of 1.5 h. The initial grain (particle) size was found to play an important role in affecting the microstructural evolution and the magnetic properties of CoFe₂O₄ powders during mechanical milling. The magnetic properties of milled CoFe₂O₄ powders showed different milling-time dependent behaviors for different precursors. Analysis based on XRD and TEM revealed the detailed microstructural evolution of CoFe₂O₄ powders during the mechanical milling. The results indicate that the milling-induced high coercivity was closely related to the high density of defects and high level of strain induced by milling. The enhanced in magnetic anisotropy was observed in large-grained samples after milling, which could be mainly due to the milling-induced stress anisotropy. In order to understand the coercivity mechanism behind the milling-induced high coercivity, we have presented detailed magnetic studies which revealed that the pinning controlled coercivity mechanism is responsible for the milling-induced high coercivity. The pinning centers could be dislocation-type defects, highly strained areas, and grain boundaries with the formation of subgrains during mechanical milling.

*Corresponding author. FAX: (65) 6776-3604. Electronic address: msedingj@nus.edu.sg

¹J. Ding, Y. J. Chen, Y. Shi, and S. Wang, *Appl. Phys. Lett.* **77**, 3621 (2000).

²Y. Suzuki, R. B. van Dover, E. M. Gyorgy, J. M. Philips, V. Korenivski, D. J. Werder, C. H. Chen, R. J. Cava, J. J. Krajewski, W. F. Peck, and K. B. Do, *Appl. Phys. Lett.* **68**, 714 (1996).

³H. W. J. Zheng, S. E. Lofland, Z. Ma, L. Mohaddes-Ardabili, T. Zhao, L. Salamanca-Riba, S. R. Shinde, S. B. Ogale, F. Bai, D. Viehland, Y. Jia, D. G. Schlom, M. Wuttig, A. Roytburd, and R.

Ramesh, *Science* **303**, 661 (2004).

⁴B. Zhou, Y. W. Zhang, Y. J. Yu, C. S. Liao, C. H. Yan, L. Y. Chen, and S. Y. Wang, *Phys. Rev. B* **68**, 024426 (2003).

⁵J. C. Slonczewski, *Phys. Rev.* **110**, 1341 (1958).

⁶H. Kronmüller, *Phys. Status Solidi B* **144**, 385 (1987).

⁷D. Givord, Q. Lu, and M. F. Rossignol, *Science and Technology of Nanostructured Magnetic Materials*, edited by G. C. Hadjipanayis and G. A. Prinz (Plenum, New York, 1991), p. 635.

⁸X. C. Kou, H. Kronmüller, D. Givord, and M. F. Rossignol, *Phys. Rev. B* **50**, 3849 (1994).

- ⁹Y. C. Wang, J. Ding, J. B. Yi, B. H. Liu, T. Yu, and Z. X. Shen, *Appl. Phys. Lett.* **84**, 2596 (2004).
- ¹⁰C. N. Chinnasamy, B. Jeyadevan, K. Shinoda, K. Tohji, D. J. Djayaprawira, M. Takahashi, R. Justin Joseyphus, and A. Narayanasamy, *Appl. Phys. Lett.* **83**, 2862 (2003).
- ¹¹H. W. Zhang, C. B. Rong, J. Zhang, S. Y. Zhang, and B. G. Shen, *Phys. Rev. B* **66**, 184436 (2002).
- ¹²A. Lisfi and C. M. Williams, *J. Appl. Phys.* **93**, 8143 (2003).
- ¹³A. Lisfi, J. C. Lodder, E. G. Keim, and C. M. Williams, *Appl. Phys. Lett.* **82**, 76 (2003).
- ¹⁴S. Nakagawa and M. Naoe, *J. Magn. Magn. Mater.* **120**, 345 (1993).
- ¹⁵S. Nakagawa, Y. Kitamoto, and M. Naoe, *IEEE Trans. Magn.* **26**, 106 (1990).
- ¹⁶B. G. Demczyk and J. O. Artman, *J. Phys. D* **24**, 1627 (1991).
- ¹⁷B. D. Cullity and S. R. Stock, *Elements of X-ray Diffraction*, 3rd ed. (Prentice Hall, Upper Saddle River, NJ, 2002), p. 401.
- ¹⁸E. F. Kneller and F. E. Lubo, *J. Appl. Phys.* **34**, 656 (1963).
- ¹⁹B. D. Cullity, *Introduction to Magnetic Materials* (Addison-Wesley, Reading, MA, 1972), p. 385.
- ²⁰J. Ding, T. Reynolds, W. F. Miao, P. G. McCormick, and R. Street, *Appl. Phys. Lett.* **65**, 3135 (1994).
- ²¹J. M. Coey, *Phys. Rev. Lett.* **27**, 1140 (1971).
- ²²D. J. Craik, *Magnetic Oxides* (Wiley, London, New York, 1975), p. 32.
- ²³B. D. Cullity, *Introduction to Magnetic Materials* (Addison-Wesley, Reading, MA, 1972), p. 387.
- ²⁴E. Hellstern, H. J. Fecht, C. Garland, and W. L. Johnson, *Materials Research Society Symposium Proceedings No. 32* (Materials Research Society, Pittsburgh, 1989), p. 137.
- ²⁵J. Y. Huang, Y. K. Wu, and H. Q. Ye, *Acta Mater.* **44**, 1211 (1996).
- ²⁶P. G. McCormick, W. F. Miao, P. A. I. Smith, J. Ding, and R. Street, *J. Appl. Phys.* **83**, 6256 (1998).
- ²⁷P. E. Donovan and W. M. Stobbs, *Acta Metall.* **31**, 1 (1983).
- ²⁸J. Karch, R. Birringer, and H. Gleiter, *Nature (London)* **330**, 556 (1987).
- ²⁹D. L. Leslie-Pelecky and R. L. Schalek, *Phys. Rev. B* **59**, 457 (1999).
- ³⁰R. Grössinger, *Phys. Status Solidi A* **66**, 665 (1981).
- ³¹V. Šepelák, U. Steinike, D. C. Uecker, S. Wibmann, and K. D. Becker, *J. Solid State Chem.* **135**, 52 (1998).
- ³²V. Šepelák, D. Baabe, F. J. Litterst, and K. D. Becker, *J. Appl. Phys.* **88**, 5884 (2000).
- ³³Y. C. Wang, J. Ding, J. H. Yin, B. H. Liu, J. B. Yi, and S. Yu, *J. Appl. Phys.* **98**, 124306 (2005).
- ³⁴B. D. Cullity, *Introduction to Magnetic Materials* (Addison-Wesley, Reading, MA, 1972), p. 258.
- ³⁵V. J. Folen, in *Magnetic and Other Properties of Oxides and Related Compounds*, edited by K. H. Hellwege and A. M. Hellwege, Landolt-Börnstein, New Series, Group III, Vol. 4, Pt. B (Springer, Berlin, Heidelberg, New York, 1970), p. 366.
- ³⁶T. D. Shen, R. B. Schwarz, and J. D. Thompson, *Phys. Rev. B* **72**, 014431 (2005).
- ³⁷P. Gaunt, *J. Appl. Phys.* **59**, 4129 (1986).
- ³⁸J. F. Liu and H. L. Luo, *J. Magn. Magn. Mater.* **94**, 43 (1991).
- ³⁹P. Gaunt and C. K. Mylvaganam, *Philos. Mag. B* **44**, 569 (1981).
- ⁴⁰U. S. Ram, D. Ng, and P. Gaunt, *J. Magn. Magn. Mater.* **50**, 193 (1985).
- ⁴¹H. Kronmüller, K. D. Dust, and G. Martineck, *J. Magn. Magn. Mater.* **69**, 69 (1987).
- ⁴²H. Kronmüller, K. D. Dust, and M. Sagawa, *J. Magn. Magn. Mater.* **74**, 291 (1988).
- ⁴³B. D. Cullity, *Introduction to Magnetic Materials* (Addison-Wesley, Reading, MA, 1972), p. 290.
- ⁴⁴H. Shenker, *Phys. Rev.* **107**, 1246 (1957).
- ⁴⁵D. Givord, M. Rossignol, and Vitoria M. T. S. Barthem, *J. Magn. Magn. Mater.* **258-259**, 1 (2003).
- ⁴⁶E. F. Wohlfarth, *J. Phys. F: Met. Phys.* **14**, L155 (1984).
- ⁴⁷P. Gaunt, *J. Appl. Phys.* **59**, 4129 (1986).
- ⁴⁸R. Street, R. K. Day, and J. B. Dunlop, *J. Magn. Magn. Mater.* **69**, 106 (1987).
- ⁴⁹J. C. Barbier, *Ann. Phys. (Paris)* **9**, 84 (1954).
- ⁵⁰X. H. Chen and P. Gaunt, *J. Appl. Phys.* **67**, 2540 (1990).
- ⁵¹G. C. Hadjipanayis and A. Kim, *J. Appl. Phys.* **63**, 3310 (1988).
- ⁵²R. Pauthenet, *Ann. Phys. (Paris)* **7**, 710 (1952).